Available online at www.sciencedirect.com

ScienceDirect

Energy Procedia 00 (2017) 000–000

Energy Procedia

www.elsevier.com/locate/procedia

9th International Conference on Applied Energy, ICAE2017, 21-24 August 2017, Cardiff, UK

# Experimental Characterization and Multiphysics Simulation of a Triple-Junction Cell in a Novel Hybrid III:V Concentrator Photovoltaic–Thermoelectric Receiver Design with Secondary Optical Element

T K N Sweet[a*], M H Rolley[a], W Li[b], M C Paul[b]*, M Gao[a] and A R Knox[b]

[a]*School of Engineering, Cardiff University, Cardiff. CF24 3AA.*
[b]*School of Engineering, University of Glasgow, Glasgow, G12 8QQ, UK*

**Abstract**

A lattice-matched monolithic triple-junction Concentrator Photovoltaic (CPV) cell (InGaP/InGaAs/Ge) was electrically and thermally interfaced to a Thermoelectric (TE) Peltier module. A SIngLe Optical (SILO) design secondary lens was bonded to the CPV-TE receiver. The hybrid SILO-CPV-TE solar energy harvesting device was electrically, thermally and theoretically investigated. The electrical performance data for the CPV cell under variable irradiance and cell temperature conditions were measured using the integrated TE module as both a temperature sensor and as a solid-state heat pump. The CPV cell was electrically characterised under Standard Test Conditions (STC) of 1000W/m$^2$ irradiance, 25$^o$C temperature and AM1.5G spectrum for comparison with literature data. Transient multiphysics simulations in ANSYS CFX 15.0 were carried out to calculate cell temperatures and to determine the short circuit current and temperature coefficient in a scaling law. The optimization was used to determine 15 model parameters for the component sub-cells within the triple-junction cell at STC with a MATLAB scaling law. The root-mean-square error in electrical currents between measurement and simulations was 0.50%.


Peer-review under responsibility of the scientific committee of the 9th International Conference on Applied Energy.

*Keywords:* Concentrator photovoltaic; triple-junction; solar cell; thermoelectric; cell temperature; secondary optical element; optimization

## 1. Introduction

Concentrator Photovoltaic technology is a utility-scale option for the generation of solar electricity in areas of high (more than 2000 kWh/m$^2$ annual) Direct Normal Irradiance (DNI). Currently cumulative global installation capacity

* Corresponding authors. Tel.: +44(0)2920870673 and +44(0)141 330 8466; fax: +44(0)141 330 2032.
*E-mail addresses:* SweetT@Cardiff.ac.uk; Manosh.Paul@Glasgow.ac.uk


Peer-review under responsibility of the scientific committee of the 9th International Conference on Applied Energy.

of CPV exceeds 370MWp (Dec 2016) [1]. Low cost concentrating optics are used to significantly increase photon flux onto a small [typically 5.5mm x 5.5mm] CPV cell. The optics concentrate sunlight (between 300x and 1000x) and homogenise photon spectral distribution increasing cell efficiency. CPV is now competitive with flat-plate crystalline Silicon Photovoltaic (PV) technologies in terms of levelized costs of electricity (LCoE) in high DNI locations. Modular CPV systems typically include dual-axis tracking to follow the sun's trajectory and maximize energy generation throughout the day. One significant benefit of CPV is the comparatively high cell and system efficiencies produced. Compound semiconductor CPV cells are structurally designed to minimize thermalisation and transmission losses. Multiple direct bandgap materials are epitaxially grown via Metal Organic Vapour Phase Epitaxy (MOVPE) or Molecular Beam Epitaxy (MBE). High purity III:V layers, with typical total thickness <10μm, have almost perfect crystallinity leading to low non-radiative losses in the CPV device. High extinction coefficients and anti-reflective coating enables effective absorption of incident solar photons (wavelength range 250-2500nm) by the cell. High charge carrier mobility and separation enables full-spectrum energy harvesting at comparatively high efficiency. Currently the world record efficiency for a multi-junction solar cell is 46.0% by Fraunhofer ISE, Soitec and CEA-LETI [1, 2]. World record III:V cell efficiencies typically increase by ~1% per year. Advanced modelling indicates realistic targets of greater than 50% cell efficiency (1000x concentration) by 2020[3]. High-volume production cell efficiencies closely follow this trend.

To maximize the concentration ratio (CR), two optical lenses are typically used, a Primary Optical Element (POE) and a Secondary Optical Element (SOE), situated adjacent to the CPV cell. A domed-shaped SIngLe Optical (SILO) lens, which encapsulates the CPV cell, was used as the SOE in this work [4]. High cell temperatures are an inevitable consequence of high irradiance conditions. The bandgap(s) of photon-absorbing layers are reduced at higher operational temperatures. A significant reduction in the voltage of the cell, and slight increase in photo-generated current, leads to an overall net reduction in maximum power production. The TE module in a CPV-TE receiver acts as both cell temperature sensor (via Voc) and as a heat pump (upon application of current) to accurately control the CPV cell temperature. The objectives are to increase power output and minimise thermal degradation of the CPV cell. The novel hybrid SILO-CPV-TE receiver was electrically and thermally measured under different irradiance and cell temperature conditions. Standard Test Conditions (STC), 1000W/m$^2$ irradiance, 25$^o$C temperature and AM1.5G spectrum conditions gave baseline CPV cell performance. Multiphysics simulation techniques were used to predict the time-dependent cell temperature based on the recorded indoor ambient temperature and TE measurements. The electric performance of a triple-junction cell based CPV system was then modelled.

## 2. Experimental.

The SILO-CPV-TE receiver was manufactured using standard cleanroom and wire-bonding techniques. The architecture of the device is given in Fig 1(a) [5]. The hybrid device's active components consisted of a 5.5×5.5mm area lattice-matched triple junction solar cell, integrated with a Marlow CM23-1.9 bismuth telluride TE module. A photograph of the device showing electrical contacts is given in Fig 1(b). A water heat exchanger and appropriate thermal interface material (TIM) was used. Temperature measurements were taken at the TE cold-side and ambient temperature using a K-type thermocouple, in conjunction with a Fluke 52II thermometer. A Closed Loop Integrated Cooler (CLIC) and temperature reference chip (Temp IC) were used for additional temperature data alongside a Forward Looking Infrared thermal imaging camera (FLiR i7) for thermal distribution measurements.

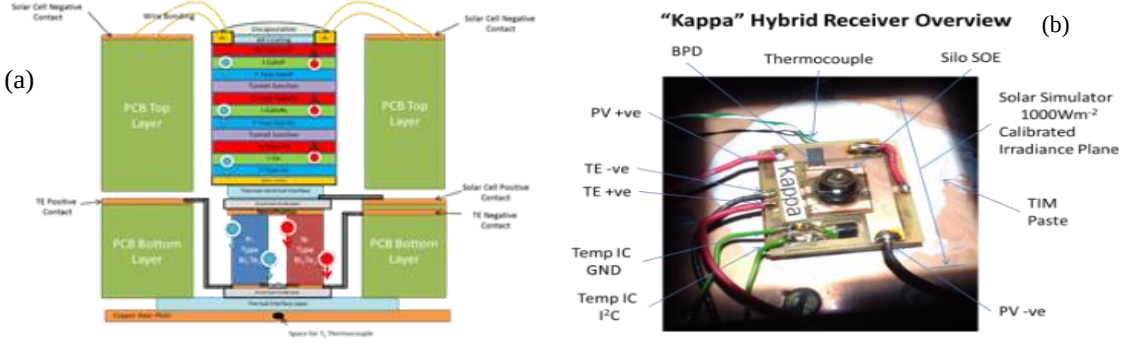


Fig.1 (a) Cross-section of CPV-TE receiver and (b) Kappa SILO-CPV-TE hybrid receiver overview.

A LOT Oriel Class ABB solar simulator was used, as shown Fig.2 (a), with the 1kW/m$^2$ calibrated irradiance plane found using a Kipp and Zohan CMP11 pyranometer. Current-Voltage (I-V) data were measured using an AUTOLAB potentiostat system, and the entirety of the experiment was conducted inside a faraday cage to eliminate any ambient light effects, Fig 2 (b). Steady-state temperatures were achieved, prior to measuring solar cell I-V curves, to eliminate changes in electrical output due to the temperature coefficient effects of the solar cell.

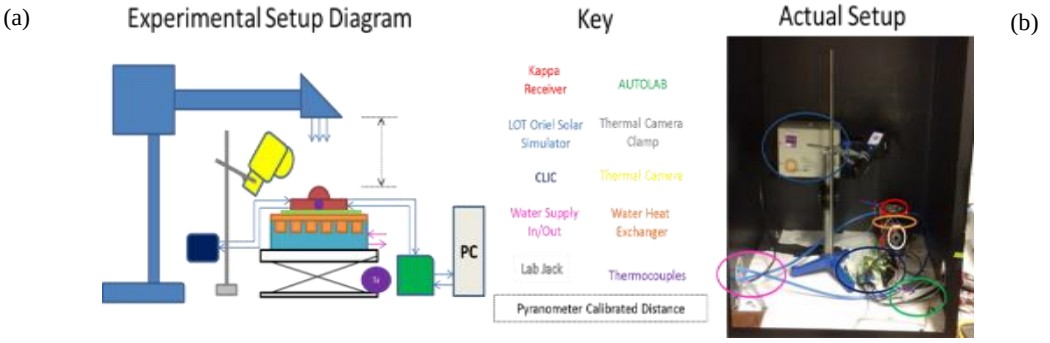


Fig.2 (a) Overview of the experimental setup and (b) Actual experimental setup in the Faraday cage.

## 3. Simulation

The computational domain consisted of air body between the solar simulator aperture (57mm×38mm) and the dome lens, dome lens itself, the cell and an epoxy TIM layer between the cell and the TE module surface, as shown in Fig.3 (a) and (b). The air body volume was defined as 57mm×38mm×159.7mm. The dome lens height was measured 10mm from apex to base. The cell (5.5×5.5mm) in Fig. 1 was simplified as one layer using an equivalent heat transfer property constant, calculated using 1D elementary conductive heat transfer formula [6]. The CFD package-ANSYS CFX 15.0 was used to carry out transient multiphysics simulations. The transient laminar fluid flow governing equations chosen were the Boussinesq approximation, natural convective heat transfer equations and grey radiative models. These were incorporated to describe the buoyancy-driven air flow between the solar aperture and the dome lens to investigate influence on cell temperature. The conductive heat transfer equations and grey radiative models were used for the dome lens and cell, while the conductive heat transfer equations were applied to the epoxy layer. The fluid flow, convective, conductive heat transfer equations were discretized using a finite volume method, and coupling between the continuity and momentum equations accomplished with the "SIMPLE" algorithm. The grey radiative equation was solved by means of a Monte Carlo method. The air body, and dome lens were discretized with tetrahedral elements, the cell and epoxy layer were discretized with hexahedrons. Three sets of meshes with 112888, 359217 and 1623711 elements respectively. The ambient and TE temperatures, recorded during the experiment, were input into CFX as a function of time. The average temperatures in the cell and dome lens were recorded by monitor expressions in the CFX Output Control. The time-step in the transient simulations was 100s, with 100 iterations in each time step, root-mean square (RMS) residual target $10^{-5}$.

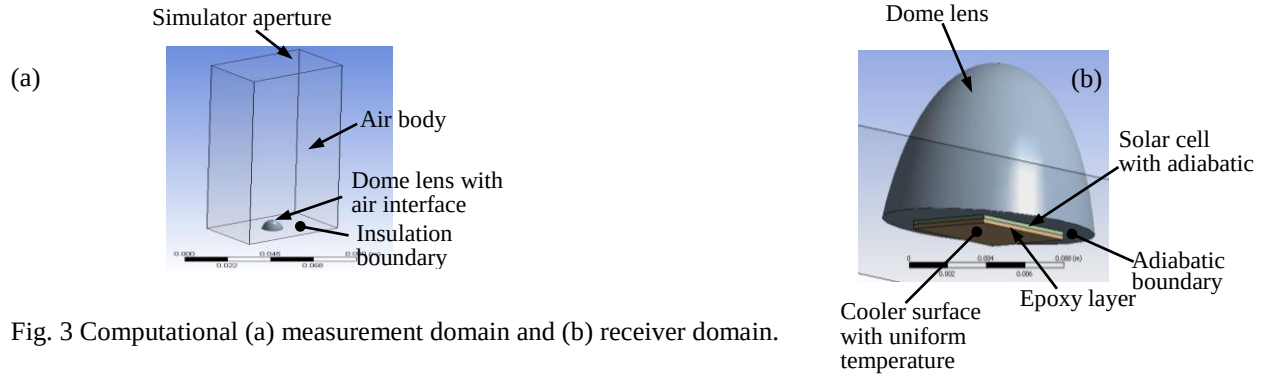


Fig. 3 Computational (a) measurement domain and (b) receiver domain.

### *3.1. Electric model*

The cell temperature may deviate slightly from the STC 25ºC at 1kW/m$^2$ irradiance. Hence, we used the model described in this paper to obtain the critical parameters to generate a simulated cell I-V curve. Existing scaling laws for solar cells show that the fifteen solar cell parameters at temperatures different to 25ºC can be found.

The shunt resistance $R_{sh}$, series resistance $R_s$ and ideality index $n$ depend on irradiance only. The short circuit current $I_{sc}$ is dependent on both the cell temperature and irradiance whereas the diode reverse saturation current $I_d$ is dependent on cell temperature alone. Therefore, under a constant irradiance, $R_{sh}$, $R_s$ and $n$ remain unchanged regardless of the cell temperature, but $I_{sc}$ and $I_d$ vary with cell temperature [7,8,9]. In this scenario, the existing scaling law was expressed by equations below (1) where subscript index $i$ =1, 2, 3 was used to denote to the top InGaP cell, middle InGaAs cell and bottom Ge cell respectively, as shown in Fig. 3.

$$\begin{cases} n_i = n_{0i}, R_{si} = R_{s0i}, R_{shi} = R_{sh0i} \\ I_{phi} = I_{sc0i} + \mu\left(T - T_0\right) \\ I_{di} = I_{d0i}\left(T/T_0\right)^3 \exp\left[\frac{1}{k}\left(\frac{Eg0i}{T_0} - \frac{Egi}{T}\right)\right], i = 1,2,3 \end{cases} \quad (1)$$

Subscript 0 is the cell operating at 25ºC STC, $\mu$ the short-circuit temperature coefficient, 2.2188×10$^{-5}$ A/K based on experimental I-V curves (Fig.5). $\kappa$ Boltzmann constant, 8.61733035×10$^{-5}$eV/K. Sub-cell temperature ($T$) at non STC conditions, $I_{phi} \approx I_{sci}$. The three sub-cells were assumed to share the same temperature. $E_{gi}$ is the band gap of the top InGaP cell [8], middle InGaAs cell [9] and bottom Ge cell [ 10 ], respectively. Under STC conditions, the I-V curve of a triple-junction solar cell can be written as (2)

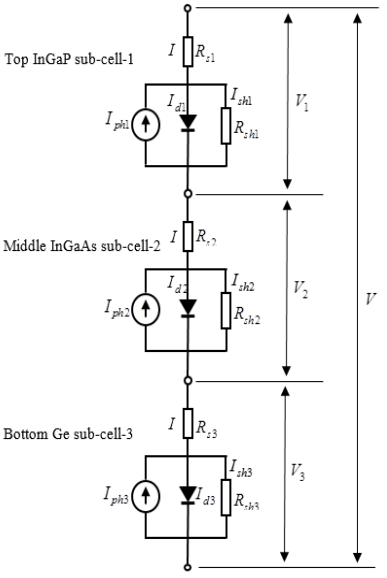


Fig.3 Lumped electric model of 3J cell

$$\begin{cases} I = \dfrac{\sum_{i=1}^{3} I_{sc0i} R_{sh0i} - \sum_{i=1}^{3} I_{d0i}\left\{\exp\left[\dfrac{q\left(V_i + IR_{s0i}\right)}{n_{0i}\kappa T_0}\right] - 1\right\} R_{sh0i} - V}{\sum_{i=1}^{3}\left(R_{s0i} + R_{sh0i}\right)} \\ V_1 = 0.5V, V_2 = 0.35V, V_3 = 0.15V \end{cases} \quad (2)$$

Where $q$ is the electron charge, $q$ =1.60217662 × 10$^{-19}$C, the Boltzmann constant is $\kappa$ =1.38064852×10$^{-23}$J/K. The second equation in Eq. (2) is based on [11]. Under an off STC condition where the cell temperature is no longer equal to 25ºC but the irradiance is kept at 1kW/m$^2$, the I-V curve of the triple-junction solar cell is expressed as (3)

$$\begin{cases} I = \dfrac{\sum_{i=1}^{3} I_{phi} R_{shi} - \sum_{i=1}^{3} I_{di}\left\{\exp\left[\dfrac{q\left(V_i + IR_{si}\right)}{n_i \kappa T}\right] - 1\right\} R_{shi} - V}{\sum_{i=1}^{3}\left(R_{si} + R_{shi}\right)} \\ V_1 = 0.5V, V_2 = 0.35V, V_3 = 0.15V \end{cases} \quad (3)$$

If the 15 model parameters $I_{sc0i}$ $I_{d0i}$, $R_{s0i}$, $n_{0i}$, $R_{sh0i}$ at STC and the scaling law, Eq. (1), are available, then the 15 model parameters $I_{phi}$ $I_{di}$, $R_{si}$, $n_i$ and $R_{shi}$ at different temperatures will be predicted. The off-STC I-V curves can then be calculated. Our task is to determine the 15 model parameters, at STC, from two sets of I-V curves at cell temperatures other than 25ºC. This inverse problem can be expressed mathematically in (4)

$$f\left[I_{sc0i}, I_{d0i}, R_{s0i}, n_{0i}, R_{sh0i}, \text{scaling law of Eq.(1)}\right] = \sum_{j=1}^{N}\left(I_j^m - I_j^e\right)^2 \to \min \quad (4)$$

Where $I_j^m$ and $I_j^e$ are the current predicted with Eq. (3) and the off STC measured current at a voltage $V_j^e$, $j$ is the index indicating an experimental data point, $N$ is the number of total experimental data points. $I_{sc0i}$ $I_{d0i}$, $R_{s0i}$, $n_{0i}$ and $R_{sh0i}$ are determined at STC by trust-region-reflective least squares algorithm (*lsqnonlin function*) in MATLAB.

## 4. Results

For proper estimation of cell temperature, a CFX transient multiphysics simulation was done, using a representative thermal contact resistance 20cm$^2$ s K/cal ($4.7801\times10^{-4}$m$^2$ K/W) between the interface of the cell and the epoxy layer. Using this correction, the temperature profile showed better agreement (Fig.5). Under this thermal contact resistance, the cell temperature was found to be 14.86ºC at a time of 60min.

For mesh1, mesh2 and mesh3, the mean cell temperatures were calculated to be 14.86, 14.59 and 14.47ºC at 60 min respectively, showing little variation (0.49ºC) even with an increased number of elements 14.3 fold from mesh1 to mesh3. Here we choose 14.59ºC to be the cell temperature and calculate the temperature influence coefficient of short current of the cel $\mu$, i.e., $\mu=\left(I_{sc2}-I_{sc1}\right)/\left(T_2-T\right)$, where $I_{sc1}$=$9.9550\times10^{-3}$ and $I_{sc2}$ =$9.7930\times10^{-3}$A at $T_1$ =22.2 and $T_2$ =14.59ºC. With these data, the temperature influence coefficient can be worked out $\mu$ =$2.1288\times10^{-5}$ A/K.

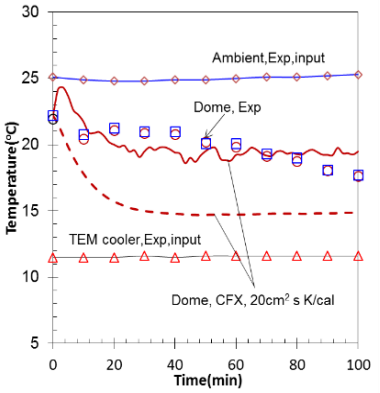


Fig.5 Input and output temperature profiles

$$\mu=\frac{I_{sh2}-I_{sh1}}{T_2-T_1} \qquad (6)$$

The I-V curves at two cell temperatures $T_1$ =22.2 ºC and $T_2$ =14.59ºC were experimentally measured. Curves were fitted to extract 15 electric model parameters at STC. Appropriate boundary conditions were used for calculation of each parameter by referring to existing results of similar triple-junction cells [12]. The resulting extracted parameters are in Table 1 and Fig 6. The calculated root-mean-square error (RMSE) of the predicted currents at two cell temperatures are compared against experimental (normalized using mean experimental Isc).

Table 1 Model Calculated parameters of three sub-cells at STC from an off-STC input

| Parameter | $R_{s0i}$ (Ω) | $R_{sh0i}$ (Ω) | $n_{0i}$ | $I_{d0i}$ (μA) | $I_{sh0i}$ (A) | RMSE (%) |
|---|---|---|---|---|---|---|
| Top InGaP cell, $i$ =1 | $9.4536\times10^{-4}$ | $7.7151\times10^{3}$ | 2.5464 | $4.9771\times10^{-5}$ | $1.1188\times10^{-2}$ | 0.50 |
| Middle InGaAs cell, $i$ =2 | $8.9391\times10^{-4}$ | $1.4158\times10^{3}$ | 2.4792 | $4.9877\times10^{-5}$ | $7.8834\times10^{-3}$ | |
| Bottom Ge cell, $i$ =3 | $9.9867\times10^{-4}$ | $1.5146\times10^{3}$ | 0.6358 | $1.4627\times10^{-5}$ | $6.3431\times10^{-3}$ | |

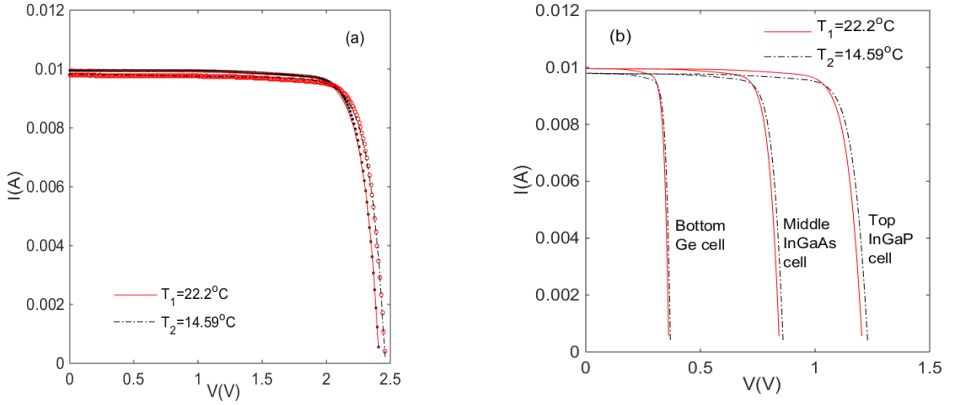


Fig.6 Comparison of measured (a) and model current-voltage I-V curves for the three sub-cells (b)

## 5. Conclusions

Novel hybrid SILO-CPV-TE receivers have been manufactured and electrically, thermally and theoretically analysed. The integrated TE module successfully acts as both a temperature sensor and as a solid-state heat pump for the CPV cell. This experimental platform can be used to accurately measure electrical current-voltage characteristics under Standard Test Conditions (1000W/m$^2$ irradiance, 25$^o$C temperature and AM1.5G spectrum).

A method for determining 15 parameters of the three component sub-cells in an InGaP/InGaAs/Ge triple-junction solar cell at STC, using experimental input data has been presented. Experimental I-V curves obtained in a solar simulator at STC and non-STC temperatures at 1kW/m$^2$ irradiance were used for ANSYS CFX 15.0 model validation, calibration and performance evaluation. The CPV cell temperature, short circuit current and temperature co-efficient within the hybrid device were calculated via a scaling law in the multiphysics simulations. The method was successfully coded in MATLAB and the 15 parameters for the component sub-cells were optimized/extracted at STC. A small error at the I-V curve 'knee', the location near the Maximum Power Point, is caused from the one-diode model adopted here. Overall the RMSE was shown to be 0.50% in electrical currents for all three sub cells, showing excellent curve fitting and validation of both the experimental methodology and the simulation model.

Future work will include installation of a primary optical element for higher optical concentration and further development of automatic sampling. The multiphysics model presented also shows potential for modification/development to analyse band gap changes related to changes in the incident solar spectrum on the CPV cell. The experimental and theoretical work presented in this paper can be used for further thermally-dependant CPV cell characterisation (both STC and non-STC) conditions. This data will be used for future hybrid CPV-TE device architectures to optimise electrical performance, device/system lifetime and LCoE reduction.

## Acknowledgements

Sêr Cymru National Research Network and the EPSRC Solar Challenge project SUNTRAP (EP/K022156/1) are gratefully acknowledged for financial support. Grateful thanks are extended to IQE plc for supply of high efficiency III-V triple-junction CPV cells, and Cardiff University School of Physics for the use of cleanroom facilities.

## References

[1] Green MA, Emery K, Hishikawa Y, Warta W and Dunlop ED "Solar cell efficiency tables (version 47) "Prog. Photovolt., Res. Appl. 24 (1), 3-11 (2016).

[2] Dimroth F, Tibbits TND, Niemeyer M, Predan F, Beutel P, Karcher C, Oliva E, Siefer G, Lackner D, Fus-Kailuweit P, Bett AW, Krause R, Drazek C, Guiot E, Wasselin J, Tauzin A and Signamarcheix T, "Four -Junction Wafer-Bonded Concentrator Solar Cells" IEEE J. Photovolt. 6 (1) 343-349 (2016).

[3] Lumb M et al, 43rd PVSEC (2016) [http://www.pvsec-26.com/pvsec-2016-singapore]

[4] James LW, Sandia National Laboratories Albuquerque, New Mexico for US Department of Energy (SAND89-7029), 1989.

[5] Sweet TKN, Rolley M, Min G, Knox A, Gregory D, Paul D, Paul M, Montecucco A, Siviter J, Mullen P, Ashraf A, Li W, Mallick T, Sellami N, Baig H, Meng X-L, Freer R, Azough F, Fernandez-Fernandez E, Scalable Solar Thermoelectric and Photovoltaics (SUNTRAP), Americal Institute of Physics, 1766, 080007 (2016).

[6] Incropera FP, Dewitt DP, Bergman TL and Lavine AS, Fundamentals of Heat and Mass Transfer, 6tt edition, 2007, Hoboken: John Willey & Sons.

[7] De Soto W, Klein SA, Beckman WA, Improvement and validation of a model for photovoltaic array performance, Solar Energy, 2006, 80, 78-88.

[8] Dongue S, Njomo D, Ebengai L, An improved nonlinear five-point model for photovoltaic modules, International Journal of Photoenergy, 2013, 11 pages.

[9] Siddiqui MU, Arif AFM, Kelly L, Dubowsky S, Three-dimensional thermal modelling of a photovoltaic module under varying condition, Solar Energy, 2012, 86, 2620-2631.

[10]O'Donnell K P and Chen X, Temperature dependence of semiconductor band gap, Applied Physics Letters, 1991, 58(25), 2924-2926.

[11]Ben Or A and Appelbaum J, Estimation of multi-junction solar cell parameters, Progress in Photovoltaics: Research and Applications, 2013, 21, 713-723.

[12] Wei J, Murray JM, Barnes J, Gonzalez L P, Guha S, Determination of the temperature dependence of the band gap energy of semiconductors from transmission spectra, Journal of Electronics Materials, 2012, 41(10), 2857-2866.